Short range attractive colloids: dynamics and energy landscape properties

2008 J. Phys.: Condens. Matter 20 075108

(http://iopscience.iop.org/0953-8984/20/7/075108)

IOP PUBLISHING JOURNAL OF PHYSICS: CONDENSED MATTER

J. Phys.: Condens. Matter **20** (2008) 075108 (10pp) doi:10.1088/0953-8984/20/7/075108

Short range attractive colloids: dynamics and energy landscape properties

Giuseppe Foffi[1,2] **and Luca Angelani**[3]

[1] Institut Romand de Recherche Numérique en Physique des Matériaux (IRRMA), Ecole Polytechnique Fédérale de Lausanne (EPFL), CH-1015 Lausanne, Switzerland
[2] Institute of Theoretical Physics (ITP), Ecole Polytechnique Fédérale de Lausanne (EPFL), CH-1015 Lausanne, Switzerland
[3] Research Center SMC INFM-CNR, c/o Università di Roma 'La Sapienza', Pizzale Aldo Moro 2, I-00185, Roma, Italy

Received 2 July 2007, in final form 29 December 2007
Published 25 January 2008
Online at stacks.iop.org/JPhysCM/20/075108

Abstract
We discuss the static and dynamical properties of a model of short range attractive colloidal systems. Our model is a binary mixture of particles interacting with a modified Lennard-Jones potential that we simulated by molecular dynamics. As previously found, we confirm the existence of a maximum in diffusivity on varying the temperature at constant high density. The possibility to characterize such a maximum by studying the properties of the potential energy landscape (PEL) is also discussed. This has been achieved by calculating the configurational entropy following two independent methods. It is shown that this quantity presents a maximum in correspondence with that of diffusivity.

(Some figures in this article are in colour only in the electronic version)

1. Introduction

In recent years the advances in colloidal science have allowed us to discover new important phenomena and to check many theoretical predictions. A typical example is represented by hard spheres. For this system, a freezing transition was predicted in the pioneering work of Hoover and Ree nearly 40 years ago [1]. For 20 years this prediction remained just a speculation until the 1980s when a first order liquid–solid phase transition, of purely entropic origin, was experimentally detected in a system of hard spheres colloids [2].

Another interesting case is represented by systems with short range attractive interactions. In molecular systems, the range of the attraction is generally much longer than the typical size of the molecules. Consequently the role of the range has never been investigated in detail. For colloidal systems, however, it is possible to have much richer interactions [3]. When a colloidal solution contains polymers with a radius of gyration much smaller than the diameter of the particles, for example, an effective attractive interaction sets in. In particular, the radius of gyration of the polymer modulates the range of such attraction. In short ranged attractive colloidal systems (SRACS) new thermodynamic behaviors emerged as predicted by theory [4] and simulations [5]. In particular, when the range of the attraction is short enough, the liquid–liquid phase separation becomes metastable with respect to the fluid–crystal one. For a recent review on SRACS see, for example, [6].

The dynamical properties of colloidal systems are also important. For hard spheres, for example, a dynamics arrest has been found when the system is prepared at high densities [7]. In this situation, the system is frozen in a disordered structure—a glass—and does not relax anymore. The existence of this colloidal glassy regime is of great importance because it has allowed the predictions of mode coupling theory (MCT) for the glass transition to be fully tested [8]. Indeed, in a set of beautiful experiments Van Megen and Underwood gave the first proof of the validity of the MCT prediction for hard spheres [9].

For SRACS, the phenomenology is even richer. When the range of attraction is a few percentiles of the colloid diameter, MCT predicts a re-entrant line in the density–temperature plane [10, 11]. This means that, above a certain density, it is possible to melt the glass by lowering the temperature, and to vitrify it again by decreasing it further. New interesting phenomena, such as higher order MCT singularities, two different type of glass and anomalous logarithmic decay in the density correlators, were also predicted [12]. The presence of a re-entrant glassy line is responsible for a maximum in

diffusivity varying the temperature along a constant density path. This phenomenon has been carefully investigated and its existence has been successfully established both in experiments and simulations [13–17].

In this paper we will discuss the possibility of relating the maximum in the diffusivity with the number of states visited by the system, i.e. with the so-called configurational entropy. For water, Scala *et al* [18] showed that this maximum, that emerges when the pressure varies, is indeed reflected in a maximum in the configurational entropy. In that case the phenomenon is related to the non-spherical feature of the potential. For SRACS, however, the interaction is centro-symmetric, and consequently the origin of the phenomenology is completely different.

To investigate this problem we choose a modification of the standard Lennard-Jones potential that mimics the short range attraction typical of SRACS. We had to choose a continuous potential instead of the discontinuous square-well potential largely studied by one of us in the past [12, 16, 17] because one of the routes to calculate the configurational entropy is the characterization of statistical properties of the potential energy landscape (PEL) [19–21] that requires the interaction to be continuous.

In this work, we first simulated the system by standard molecular dynamics (MD) at a given density. From these simulations, we calculated the static and dynamical quantities for different temperatures. In particular, we showed that the system has a maximum in diffusivity. Next, the maximum in the diffusivity was connected to the configurational entropy of the system following two independent routes. The aim of the paper is two-fold, on one hand we shall provide further details on the calculation of the configurational entropy as calculated in [22] and on the other we shall discuss the static and dynamical properties of the colloidal model we chose to investigate.

The paper is organized as follow. In section 2 we will introduce the model and discuss the details of the simulations. In section 3 we shall study the statics and dynamics of the system as well as the behavior of the diffusivity. Finally, section 4 will focus on the calculation of the configurational entropy.

2. The model

The particles interact by a generalization of the Lennard-Jones pair potential

$$V_{\mathrm{LJ}n}(r) = 4\epsilon\left[\left(\frac{\sigma}{r}\right)^{2n} - \left(\frac{\sigma}{r}\right)^{n}\right] \tag{1}$$

with $n = 100$. This value of n gives rise to a very short range interaction with respect to the diameter of the particles σ. This model potential [23] is a sort of continuous version of the 3% square-well potential V_{sw} that has been used as an effective short range potential for attractive colloids [16, 17]. In figure 1 $V_{\mathrm{LJ}n}$ is shown together with discontinuous V_{sw}. We simulated $N = 256$ particles enclosed in a cubic box with periodic boundary conditions. We have studied a binary mixture with two types of particle, A and B, with the same mass and at the same concentration. The potential parameters are $\sigma_{\mathrm{AA}}/\sigma_{\mathrm{BB}} = 1.2$, $\sigma_{\mathrm{AB}} = (\sigma_{\mathrm{AA}} + \sigma_{\mathrm{BB}})/2$ and $\epsilon_{\mathrm{AA}} = \epsilon_{\mathrm{BB}} = \epsilon_{\mathrm{AB}}$. With this choice the system does not show any sign of crystallization. We use Lennard-Jones units (σ_{AA} for length, ϵ_{AA} for energy and $\tau = (m\sigma_{\mathrm{AA}}^2/\epsilon_{\mathrm{AA}})^{1/2}$ for time). The Boltzmann constant k_{B} was set to unity, consequently the temperature is measured in units of ϵ_{AA}. Cut and shift in the pair potential are used ($r_{\mathrm{cut}} = 1.4$). Since the potential is extremely narrow, we have chosen a particularly short time ($t_0 = 7 \times 10^{-5}$) step to guarantee energy conservation. Using isothermal molecular dynamics with a Noose–Hoover thermostat [24], we investigate many temperatures between 0.26 and 2.0 at a density $\rho = N/V = 1.43$, corresponding to the packing fraction $\phi = \frac{\pi}{6}(N_{\mathrm{A}}\sigma_{\mathrm{AA}}^3 + N_{\mathrm{B}}\sigma_{\mathrm{BB}}^3)/V = 0.59$. The 5×10^7 steps have been used to equilibrate the system. The data were acquired during the following 2.1×10^8 steps. For the slower systems, two independent samples were used to reduce the statistical error.

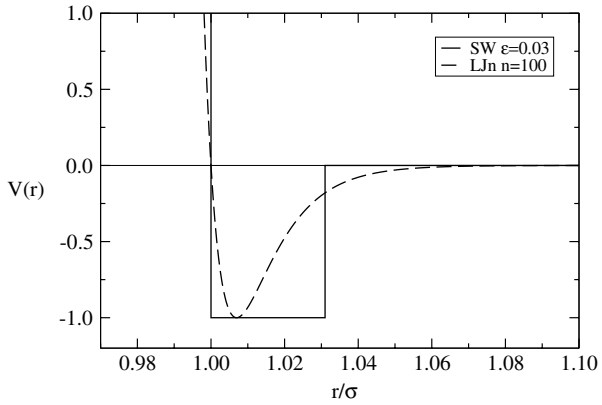

Figure 1. Pair potential $V_{\mathrm{LJ}n}$, with $n = 100$, together with an equivalent square-well with range $\epsilon = 0.03$.

3. Static and dynamic properties

As discussed in the introduction, short ranged attractive potentials present several peculiar dynamical behaviors at high densities, the most striking of these being the presence of a re-entrant glass transition and the existence of two distinct glassy phases, whose origin is driven either by attraction or by repulsion. Historically, the first hint of these new interesting features came from MCT calculations for a system of interacting particles by Yukawa [25] and the Baxter potential [10]. Later the effect of the range was systematically investigated for a square-well system [12]. Today, the presence of a re-entrance in the glass line for a short range potential has been demonstrated both in experiments and numerical simulations. Indeed these findings represented one of the most striking successes of MCT.

The model we discuss here, being characterized by a short ranged attraction, should present all the properties discussed above. In particular, keeping fixed the density and varying the temperature, a maximum should appear in the diffusion constant.

In this section we will carefully discuss some of the static and dynamic properties of the $V_{\mathrm{LJ}n}$ potential as obtained by MD simulations. First we will focus on static quantities, i.e. the static structure factors and the radial distribution functions. The partial static structure factor $S_{\alpha\beta}(q)$ is defined by

$$S_{\alpha\beta}(q) = \frac{1}{N}\langle \rho_\alpha(-q,0)\rho_\beta(q,0)\rangle \tag{2}$$

where $\alpha(\beta) = A, B$ and $\rho_\alpha(\mathbf{q},t) = \sum_l \exp(\mathrm{i}\mathbf{q}\cdot\mathbf{r}_l^{(\alpha)}(t))$ is the density variable for the species α. These quantities have been calculated by averaging over up to 300 independent q-vectors with the same modulus and for several independent equilibrated configurations; consequently the statistical error, due to the small number of particles considered, is noticeably reduced. This quantity is directly related to Fourier transform of the radial distribution function, $g_{\alpha\beta}(r)$, that has also been numerically evaluated. We focused on the packing fraction $\phi = 0.59$ and we studied 16 temperatures ranging from 0.25 up to 2.0. As we shall discuss later, this is indeed the range of temperatures where the maximum density is encountered. We verified that the dynamics between the two species does not decouple, and consequently we shall focus only on the properties of species A, since for species B the results are similar.

The partial static structure factors are presented in figure 2(a). One observes that the shape of the structure factor changes monotonically as a function of temperature. In particular, on decreasing the temperature the height of the first peak decreases whereas its width grows (see the inset of figure 2(a)). This effect is mainly due to the attraction that strengthens the bonds between particles, as it can be argued by the radial distribution function (figure 2(b)) which shows that the particles at low temperatures spend more time closed together. On the contrary, at high temperature the first coordination shell gets looser. As we shall see in what follows this is a clear indication of the different origin of the kinetic slowing. Indeed, the system has a tendency to form bonds which are stronger the lower the temperature and this increases the relaxation time. On the other hand at high temperatures each particle starts to feel its neighbors and this strongly affects the dynamics; it is the so-called cage effect. A maximum in diffusivity arises from competition between these two effects. In general, we find that the behavior of the static structure factor is in agreement with other short range attractive potentials studied previously [16, 26] and this guarantees that, for the present model, the dynamical properties are also a result of the competition between attraction and repulsion.

We shall now turn to the dynamical properties. The first quantity that we will take into account is the mean square displacement (MSD), $\langle r^2(t)\rangle = N^{-1}\langle[\mathbf{r}(t) - \mathbf{r}(0)]^2\rangle$, where $\mathbf{r}$ is the vector of the coordinates. Within Newtonian dynamics, the behavior of the MSD at short times follows the simple law $\langle r^2(t)\rangle \sim t^2$, which accounts for the ballistic motion of the particles. At later times, particles start to feel the presence of each other and there is a crossover to the diffusive regime, i.e. $\langle r^2(t)\rangle \sim t$. The diffusion coefficient D is defined by the celebrated Einstein relation [27],

$$\lim_{t\to\infty} \frac{\langle r^2(t)\rangle}{t} \simeq 6D. \tag{3}$$

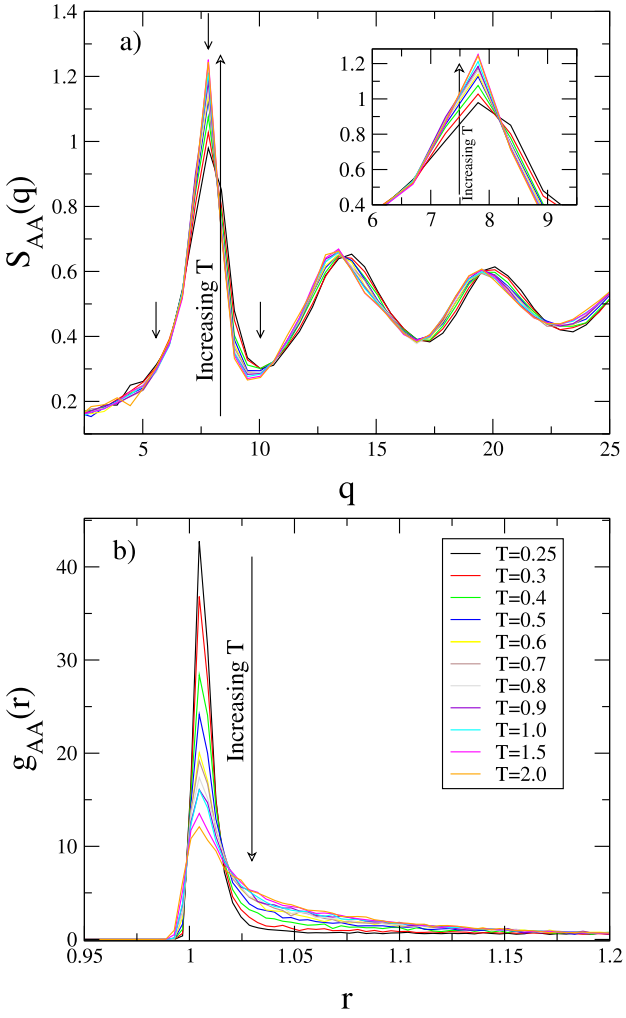

Figure 2. Static structure factors $S_{\mathrm{AA}}(q)$ (a) and radial distribution functions $g_{\mathrm{AA}}(r)$ (b) of species A particles for all the temperatures studied. Arrows in the panel (a) correspond to three different q vectors used in the calculation of the intermediate scattering function (see figure 4).

Thus, from the long time limit of the MSD, we determined the diffusion coefficient D for each state point. At this point it is perhaps worth saying few words about the choice to use Newtonian dynamics instead of Brownian dynamics. As a matter of fact, the latter represents a more realistic choice since it models the interaction of the colloidal particles with the molecules of the solvent. It has been shown, however, that the structural relaxation dynamics is independent of the short time dynamics [28]. Concerning MCT prediction on the glass transition, it has also been shown that the relaxation dynamics do not depend on the microscopic dynamics [29]. More recently, it has also been shown that in the aging process of a gel model the results are not dependent on the microscopic dynamics [30]. Consequently we decided to use Newtonian dynamics since it allows us to span much longer times by computer simulations. In figure 3 the MSD is displayed for the different temperatures we studied. In particular in figure 3(top) we present the MSD for species A, for $T \leqslant 0.5$. This is the regime where the attraction starts to dominate. At

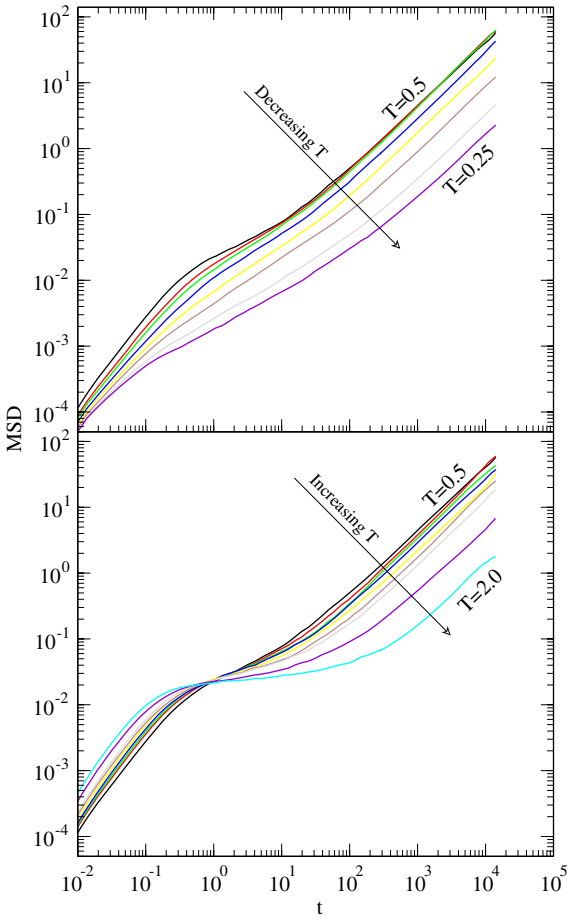

Figure 3. Mean square displacements of type A particles for all T (the legend is the same as in figure 2). Top: data for $T < 0.5$. Bottom: data for $T > 0.5$.

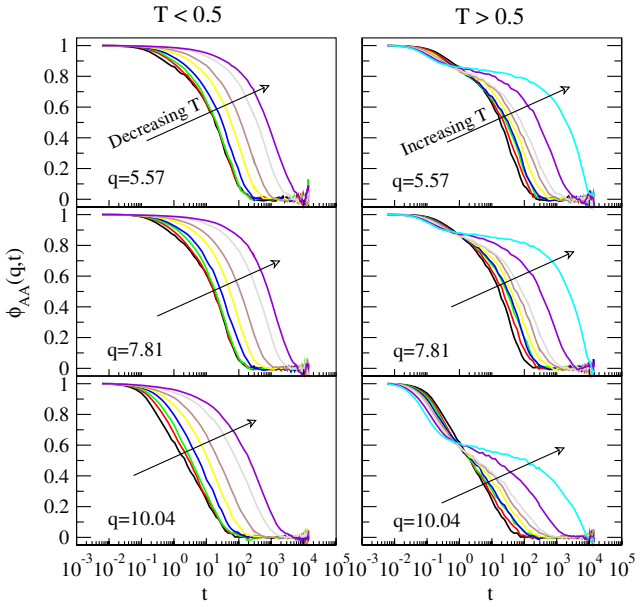

Figure 4. Left: density–density correlation functions for three representative q-vectors (see figure 2) and $T \leqslant 0.5$. Right: same as in the left panel but for $T > 0.5$.

$T = 0.5$ a first hint of structural slowing down is present as a plateau at $\langle r^2(t)\rangle \sim 0.02, 0.03$, which is the typical length scale squared for the rattling inside a first neighbor cage. On lowering the temperature, however, this plateau tends to disappear and the dynamics get slower. According to the MCT calculation, in this attractive regime a plateau at a much shorter length scale should start to emerge. This would be an indication that the particles get localized within the attractive well rather then inside a neighboring cage. Nevertheless, only a first hint of this plateau is observed. This agrees with the observation that the attractive glass is not stable for square-well systems [17], even if a deep quench at low temperature is performed. This is due mainly to activated processes that tend to destabilize the energetic bonds between particles. Recently, however, indications of the existence of such a plateau for a completely different attractive system tailored with a long repulsive barrier has been discussed [31]. In figure 3(bottom) the MSD is presented for $T \geqslant 0.5$, i.e. the regime where repulsion is responsible for the kinetic slowing down. In this case, on increasing the temperature, the formation of a plateau at $\langle r^2(t)\rangle \simeq 0.02$ is a clear indication of the cage effects and the length of the plateau grows as the time that a particle spends trapped by its neighbors increases. As expected, the height of the plateau is compatible with the value obtained for square-well binary polydisperse hard sphere systems [32]: differently from the previous case, here no activated processes take place and the phenomenology follows MCT predictions more closely.

Another important quantity that can be evaluated is the density–density correlation function, or intermediate scattering function. This quantity is defined as:

$$\phi_{\alpha\beta}(q,t) = \frac{S_{\alpha\beta}(q,t)}{S_{\alpha\beta}(q)} = \frac{\langle \rho_\alpha(-q,t)\rho_\beta(q,0)\rangle}{\langle \rho_\alpha(-q,0)\rho_\beta(q,0)\rangle} \qquad (4)$$

where $\rho_\alpha(\mathbf{q},t) = \sum_l \exp(i\mathbf{q}\cdot\mathbf{r}_l^{(\alpha)}(t))$ is the density variable for species α and $S_{\alpha\beta}(q)$ are the partial static structure factors of the system, as defined by equation (2). To calculate these quantities we perform an average over up to 300 independent q-vectors with the same modulus and on several independent time windows, consequently the statistical error, due to the small number of particles considered, is noticeably reduced. We chose to focus on three representative values for the q-vectors, $q = 5.57, 7.81$ and 10.04 which are below, at and above the first peak of the static structure factors, respectively (see the arrows in figure 2). In the left panel of figure 4, we present the results for the three q-vectors in the range $T \leqslant 0.5$. On decreasing the temperature the relaxation time of the density fluctuations grows and for the lowest temperature, i.e. $T = 0.25$, it increases by almost two orders of magnitude with respect to $T = 0.5$. As discussed for the MSD, no evidence of a clear plateau emerges as a consequence of the effect of hopping processes. Another important MCT prediction for short range attractive potentials is the presence of higher order singularities [12], which have a strong influence on the dynamics [8, 33]. Indeed, in the proximity of the so-called A_4 singularity, the density–density correlation function is expected to show an unusual logarithmic decay. Evidence

of this dynamical feature has been encountered in numerical simulations [16, 17] as well as in experiments [34]. For the three q-vectors considered here there is no sign of logarithmic decay. In order to completely rule out this possibility, we also considered higher q values where the phenomenon, if present, is expected to be more relevant [35]. In our case, however, there was no evident sign of a logarithmic decay emerging up to $q = 39.05$, probably because we are not close enough to the singularity. In the right panel of figure 4, the correlators at $T \geqslant 0.5$ are presented at the same values of the q-vector discussed above. As expected from the results for the MSD, the increase in the temperature slows the system down when it starts to feel the influence of the repulsion, i.e. the cage effect. Since no activated processes are present in the repulsive glass, a clear plateau emerges as the temperature increases. This is a clear indication that the particles spend some time trapped within the cage of their neighbors and that such time increases as the temperature is raised. As expected, the height of the plateau diminishes as q gets larger.

From the density–density correlation function we can extract the relaxation time τ_{AA}, which we define from the relation $\phi_{AA}(q, \tau_{AA}) = 0.4$, and we can use equation (3) to fit the MSD to obtain the value of the diffusivity D. The two quantities are displayed in figure 5. The relaxation time (figure 5(a)) presents a minimum at $T \simeq 0.5$ and, as expected, decreases with q. This comes as no surprise since larger length scale density fluctuations take more time to relax. The diffusion constant (figure 5(b)) is normalize by the quantity $D_0 = \sigma_{AA}\sqrt{T/m_A}$ to take into account the T dependence of the microscopic time. As expected, the diffusion presents a maximum in temperature at $T \simeq 0.4$ (very close to the minimum of τ) as the effect of the competition between the attractive and the repulsive glass dynamics. It is interesting to note that, for the low temperature branch of the curve, i.e. $T < 0.4$, the diffusion drops dramatically over a relatively short range of temperature, whereas in the high temperature region the dependence on the temperature is smoother. This is due to the particular orientation of the two glassy lines in the ϕ–T plane: almost horizontal in the case of the attractive line, vertical for the repulsive one. This dependence is altered if the attraction is measured in inverse temperature $1/T$ as in other numerical works [15].

A typical effect that MCT cannot predict is the decoupling between the timescale of the diffusivity of the density fluctuations. Indeed MCT predicts that the two quantities follow a power law in such a way that the product $D \cdot \tau$ is a constant. To verify this hypothesis, we plot this product in the inset of figure 5(b). As expected, this quantities is a constant only far from the glass transition, indicating the violation of the Stokes–Einstein relation, a fact that has also been observed in other systems [36, 37]. The analysis on the dynamics that we discussed in the present section indicates that the model we choose follows the expected trends of other SRACS and possesses a diffusivity maximum. This makes it a good candidate for investigating the relation between the diffusion maximum and configurational entropy, a task that we shall tackle in the following section. The fact that the static and dynamic quantities discussed in this section do not differ from those of other SRACS allows us to conclude that all the properties we shall discuss for the configurational entropy originate from the same mechanisms.

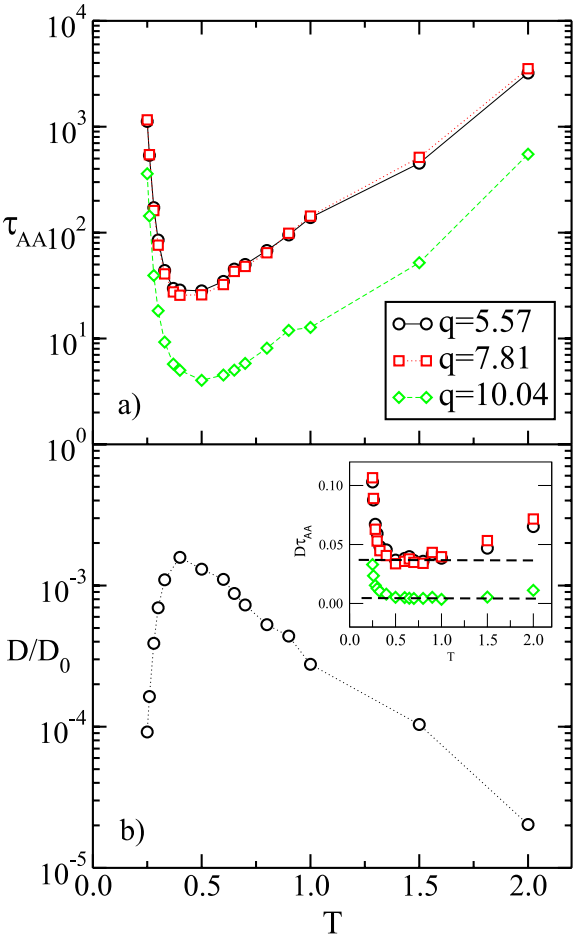

Figure 5. (a) Relaxation times $\tau_{AA}(q)$, as extracted from the correlators ϕ_{AA}, for three representative q-vectors. (b) Self diffusion constant D/D_0 determined by the mean square displacements. The inset shows the Stokes–Einstein relation, $D\tau$ versus T.

4. Configurational entropy

Configurational entropy S_{conf} is a basic quantity in the description of disordered systems, i.e. in those systems having an exponentially large number of states. It is well established that S_{conf} is not only deeply related to the possible existence of a thermodynamic transition in glassy systems (defined by the point at which S_{conf} vanishes), but also has a close relationship with the dynamics of the system, through the celebrated Adam–Gibbs relation. The calculation of S_{conf} is then of particular relevance in the study of systems with glassy behaviors, especially when, as in the present case, the system has very peculiar properties. In this section we want to answer a specific question. Is the observed diffusivity maximum related to a configurational entropy maximum? In other words, is the slowing down at high and low T signaled by a decreasing number of accessible states? To answer these questions, we have calculated the configurational entropy of

the present model using two different techniques, one based on PEL concepts and the other, more general, based on a perturbed Hamiltonian. Both make use of a decomposition of the total entropy S into a sum of a configurational contribution $S_{\rm conf}$ and a vibrational one $S_{\rm vib}$:

$$S = S_{\rm conf} + S_{\rm vib} \tag{5}$$

which comes from the idea that, close to the arrested region, there are two well separated time scales, a fast one, related to the motion inside a local state, and a slow one associated with the exploration of different states. In this section we will discuss the details of the calculation of the two terms, S (total entropy) and $S_{\rm vib}$ (vibrational entropy), needed to estimate $S_{\rm conf}$ through equation (5).

4.1. Total entropy

Let us start with the calculation of the total entropy S. We need the value of S at $\phi = 0.59$ for different values of the temperature. The standard technique consists of performing a thermodynamic integration starting from the limit of infinite dilution. In this limit the system behaves as an ideal gas and the value of the entropy is known. The integration scheme is represented schematically in the inset of figure 6(a). The first part of the path is along an isotherm characterized by $T_0 = 0.4$, starting from a density $\rho_0 = 0$ which represents the ideal limit (the point labeled A in the inset) to a density ρ which is the number density equivalent to $\phi = 0.59$. Along this isotherm it is possible to calculate the entropy at the point (T_0, ρ) (labeled B in the inset) by a thermodynamic integration:

$$S(T_0, \rho) = S^{\rm id}(T_0, \rho) + \frac{\Delta U(T_0)}{T_0} - \frac{N}{T_0}\int_0^{\rho} \frac{{\rm d}\rho'}{\rho'^2} P_{\rm ex} \tag{6}$$

where $\Delta U(T_0)$ is the variation of the energy between states A and B, $P_{\rm ex}$ is the excess pressure and $S^{\rm id}$ is the entropy of the ideal gas. For a binary mixture, the entropy of the ideal gas is

$$S^{\rm id}(T, \rho)/N = \tfrac{5}{2} - \ln\rho - 3\ln\lambda + \ln 2 \tag{7}$$

where $\lambda = (2\pi\beta\hbar^2/m)^{\frac{1}{2}}$ is the de Broglie wavelength and the term $\ln 2$ takes into account the mixing contribution due to the existence of two species rather than one. To perform the integration along this first path we proceeded numerically. We selected about 15 configurations with the volume increased logarithmically from 7030.03 (corresponding to $\phi \simeq 0.01$) to 178.55 (corresponding to $\phi = 0.59$). After a constant temperature equilibration at $T_0 = 0.4$, we calculate $P_{\rm ex}$ averaging over many independent configurations generated by simulating the system at constant energy. No sign of phase separation was encountered along this path. The values of the excess pressure obtained by this procedure are plotted in figure 6(a). In order to proceed with the integration we fitted our data with a virial expansion:

$$P_{\rm ex} = \sum_{i=2}^{m} \frac{c_i}{V^i} \tag{8}$$

where we chose $m = 7$. For the case $m = 2$, the c_2 can be calculated analytically but the agreement with the numerical

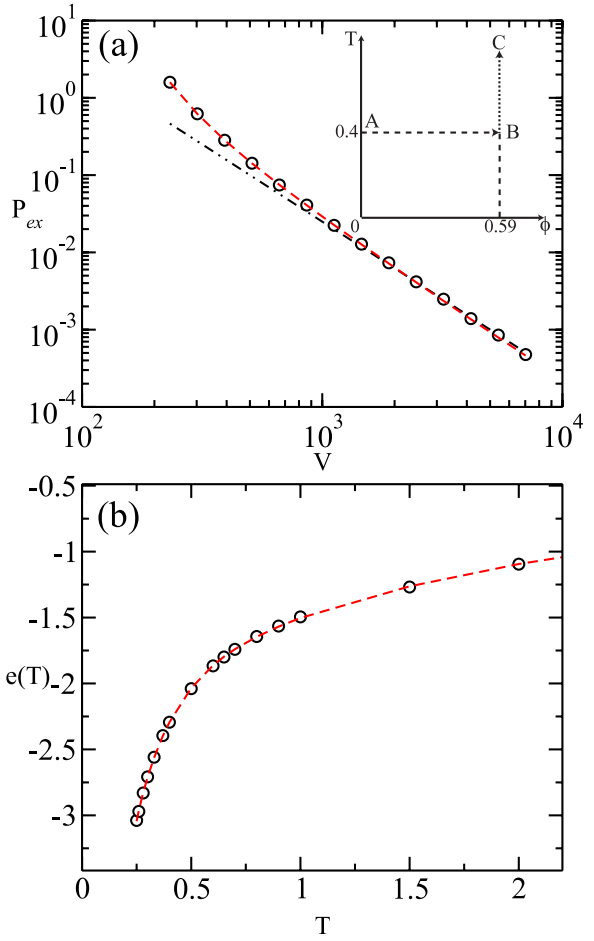

Figure 6. (a) Pressure as a function of the volume along the isotherm $T = 0.4$. The dashed line is the fit with equations (8) with $m = 7$. The dot–dot–dashed line is the fit with $m = 2$ using the analytical second virial coefficient. (b) Potential energy per particle along a constant density path, the dashed line is the fit used in the thermodynamic integration. Inset: integration path to calculate the total entropy.

data is satisfactory only at low densities. In figure 6(a), we present the results of our fits which are quite satisfactory. As expected, in the large volume limit the pressure goes to the correct limit, i.e. $P_{\rm ex} \sim 1/V^2$, which is the expansion up to the second virial coefficient [38]. Once the coefficients of the expansion (8) have been determined, the entropy of point B can be easily evaluated by performing the integral in equation (6).

The next step consists of a thermodynamic integration along a path at constant density (represented by the line (B, C) in the inset of figure 6(a)). The total entropy at different temperatures T can be evaluated by

$$S(T, \rho) = S(T_0, \rho) + \int_{T_0}^{T} \frac{{\rm d}T'}{T'}\left(\frac{3}{2}N + \frac{\partial U}{\partial T'}\right), \tag{9}$$

where $S(T_0, \rho)$ has been calculated in the (A, B) segment of the thermodynamic integration by equation (6). The internal energy per particle U/N has been extracted by the MD run at the temperature of interest and the result is shown in figure 6(b). To perform the integral in equation (9), we fit the potential energy per particle $e(T) = U(T)/N$ with a

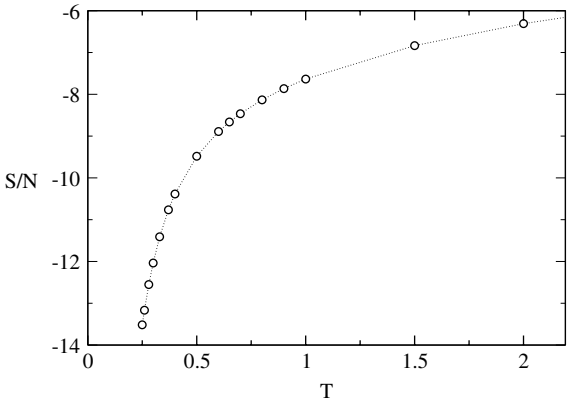

Figure 7. Total entropy as a function of temperature at constant $\phi = 0.59$.

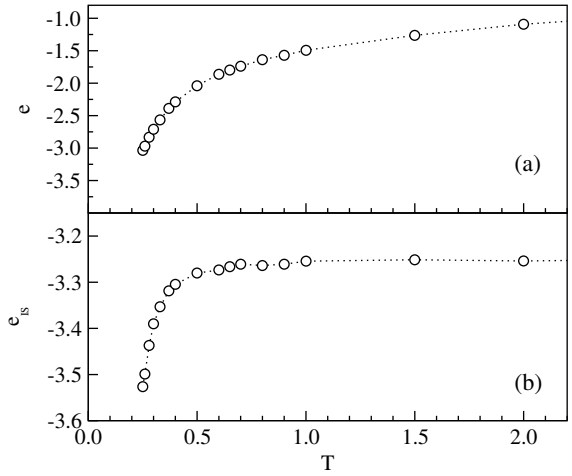

Figure 8. (a) Average energy and (b) inherent structure energy as a function of temperature.

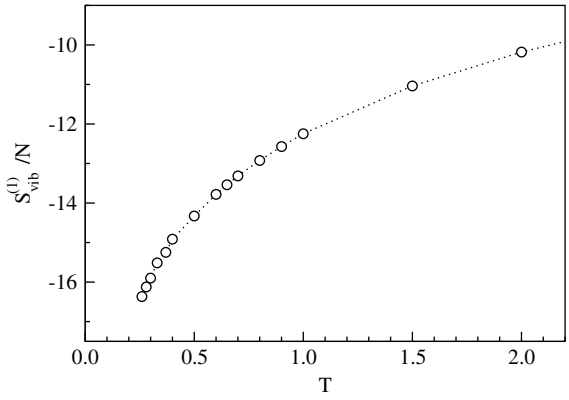

Figure 9. PEL vibrational entropy as a function of temperature.

proper functional form. In previous works [39], the functional form $e(T) = b_0(\rho) + b_1(\rho)T^{3/5}$ proposed by Rosenfeld and Tarazona [40] has been successfully used. In our case, however, this law does not seem to hold, probably due to the particular form of the potential. Consequently we interpolate the data with a simple polynomial model. The result of the interpolation is displayed in figure 6(b). With this interpolating function, we can now easily perform the integral in equation (9) and obtain the total entropy $S(T, \rho)$ for all the temperatures we are considering. In figure 7 the total entropy per particle at $\phi = 0.59$ is plotted as a function of temperature T.

4.2. Vibrational entropy

The second step towards the determination of $S_{\rm conf}$ is the calculation of the vibrational entropy $S_{\rm vib}$. We followed two independent routes. The first, based on PEL properties, relies on the calculation of the vibrational contribution, in the harmonic approximation, around inherent structures visited by the system. The second one, based on a perturbed Hamiltonian, implies calculating the mean square distances from a given equilibrium configuration and performing an integral over the strength of such perturbation.

4.2.1. PEL approach. In the *PEL approach*, the vibrational entropy can be calculated from local curvatures of the PEL around the explored inherent structures [41–45]. At each temperature we analyzed the properties of the PEL minima visited by the system during its dynamic evolution. The T-dependence of the inherent structures energy $e_{\rm IS}$ is reported in figure 8(b). It can be seen there is a nearly constant value above a given temperature ($T \simeq 0.5$), similar to what has been observed in other supercooled liquids. For comparison, in figure 8(a) we also present the instantaneous energy $e(T)$. By a diagonalization procedure of the Hessian matrix we obtain information about the eigenfrequencies ω_i of the local minima. Then we can calculate the vibrational entropy in the harmonic approximation (using simple Gaussian integrations):

$$S^{(1)}_{\rm vib}(T) = \sum_{i=1}^{3N-3} [1 - \ln(\beta\hbar\omega_i)], \tag{10}$$

where $\hbar$ is Plank's constant, $\beta = 1/k_{\rm B}T$. The quantity $S^{(1)}_{\rm vib}$ is shown in figure 9, as a function of temperature.

4.2.2. Perturbed Hamiltonian approach. The second method for the calculation of $S_{\rm vib}$ is based on the Ladd–Frenkel method. It is based on the introduction of a perturbation in the original Hamiltonian [46, 47]. This method is adequate in those cases in which strong anharmonicity effects are relevant or when a direct PEL analysis is not feasible (as, for example, in the case of hard spheres [48] or square well [49, 50] potentials). One considers a new Hamiltonian H' of the following type:

$$\beta H' = \beta H + \alpha N(\mathbf{r} - \mathbf{r}_0)^2, \tag{11}$$

where

$$(\mathbf{r} - \mathbf{r}_0)^2 = \frac{1}{N}\sum_{i=1}^{N}(\vec{r}_i - \vec{r}_{0,i})^2, \tag{12}$$

H is the original Hamiltonian, α is the strength of the perturbation and $\vec{r}_{0,i}$ is the position of the i th particle taken from a given equilibrium reference configuration. We note that the new Hamiltonian depends on temperature (besides the

trivial factor α) through the T-dependence of the reference configuration $\mathbf{r}_0$, chosen among the equilibrated unperturbed configurations at temperature T. The idea is to estimate the vibrational free energy (and then the vibrational entropy) of the unperturbed Hamiltonian making an integration over the strength α of the perturbation. More specifically, we are interested in the calculation of the unperturbed free energy $F(\alpha \to 0)$. For practical purposes we use a finite value of the strength of the perturbation (α_0) instead of exactly $\alpha = 0$, due to the fact that we are interested in calculating the vibrational properties inside local minima. Hence we require that the system never escapes toward different local structures, as happens when the strength α becomes small enough. In the opposite limit, $\alpha \to \infty$, the system is an Einstein crystal, for which an analytical expression for the free energy exists

$$\beta F(\alpha_\infty) = 3N \ln \lambda + \beta E_0 + \frac{3N}{2} \ln(\alpha_\infty/\pi) \qquad (13)$$

where E_0 is the potential energy of the reference configuration $\mathbf{r}_0$ and λ is the thermal de Broglie wavelength $\lambda = (2\pi\beta\hbar^2/m)^{1/2}$. Making use of the thermodynamic relation

$$\frac{\partial(\beta F)}{\partial \alpha} = N\langle(\mathbf{r} - \mathbf{r}_0)^2\rangle_\alpha, \qquad (14)$$

where $\langle\cdots\rangle_\alpha$ is the canonical average for a specified α, we obtain, by integration, the following expression for the free energy difference between two different α values (α_∞ and α_0):

$$\beta F(\alpha_\infty) - \beta F(\alpha_0) = N \int_{\alpha_0}^{\alpha_\infty} \mathrm{d}\alpha' \langle(\mathbf{r} - \mathbf{r}_0)^2\rangle_{\alpha'}. \qquad (15)$$

If a small α_0 value can be chosen in such a way that the corresponding system is equivalent to the original system, but constrained to explore only the phase space of one state, the estimate of $\int_{\alpha_0}^{\alpha_\infty} \mathrm{d}\alpha' \langle(\mathbf{r} - \mathbf{r}_0)^2\rangle_{\alpha'}$ is sufficient to evaluate the required vibrational free energy. Finally we obtain the expression for the vibrational entropy, writing the free energy as a sum of a potential energy term and an entropic term, $\beta F(\alpha_0) = \beta E_0 + 3N/2 - S_{\mathrm{vib}}$:

$$\frac{S^{(2)}_{\mathrm{vib}}(T)}{N} = \int_{\alpha_0}^{\alpha_\infty} \mathrm{d}\alpha' \langle(\mathbf{r} - \mathbf{r}_0)^2\rangle_{\alpha'} - \frac{3}{2} \ln\left(\frac{\alpha_\infty \lambda^2}{\pi e}\right), \qquad (16)$$

where e is the Neper number. We use isothermal molecular dynamics with Hamiltonian H' to calculate $\langle(\mathbf{r} - \mathbf{r}_0)^2\rangle_\alpha$ at different α and T. We perform averages over 20 different reference configurations $\mathbf{r}_0$, chosen from equilibrated configurations with an unperturbed Hamiltonian H at temperature T. Figure 10 shows $\langle(\mathbf{r} - \mathbf{r}_0)^2\rangle_\alpha$ as a function of α for different T. The dashed line is the (T independent) high α limit, $3/(2\alpha)$. As discussed above, one has to choose an α_0 value in equation (16) in such a way that the system remains trapped in a given local state. While at high temperature the data are smooth and the values of $\langle(\mathbf{r} - \mathbf{r}_0)^2\rangle_\alpha$ remain well below the cage value (about $r^2 \simeq 2 \times 10^{-2}$, as can be extracted by the MSD; see figure 2), at low T the behavior is quite different: starting from high α, we observe first an approach to a small value $r^2 \simeq 2 \times 10^{-3}$ (corresponding to more or less the same behavior in the mean square displacement, even if less pronounced; see figure 2) and then a departure from it at smaller values of α. We interpret the former as the vibrational motion inside the state. The full line in figure 10 is a guide to the eyes that extrapolates the first behavior at lower α for the $T = 0.26$ case. We have then chosen as α_0 in equation (16) a value for which the system has not yet left the line: $\alpha_0 = 5 \times 10^2$ (indicated by a vertical line in figure 10). Although this is a feature only of the low T data, we have chosen the same α_0 for the estimation of $S^{(2)}_{\mathrm{vib}}$ for all T, in order to obtain a coherent definition of it. Moreover, in order to take into account the remaining part of the curve (from 0 to α_0) contributing to $S^{(2)}_{\mathrm{vib}}$, an extra term has been added to equation (16). In a previous study this was a constant term $c = 0.4$ for all temperatures added to the expression of $S^{(2)}_{\mathrm{vib}}$ (circles in figure 11). Here instead we give an improved estimation adding a T-dependent term, given by $\alpha_0 \langle(\mathbf{r}-\mathbf{r}_0)^2\rangle_{\alpha_0}$ corresponding to a constant *plateau* of the $\langle(\mathbf{r}-\mathbf{r}_0)^2\rangle$ from 0 to α_0 (squares in figure 11). α_∞ has been fixed at 2×10^6, where $\langle(\mathbf{r} - \mathbf{r}_0)^2\rangle_\alpha$ has reached the asymptotic behavior (dashed line in figure 10). The resulting $S^{(2)}_{\mathrm{vib}}$ as a function of T is reported in figure 11.

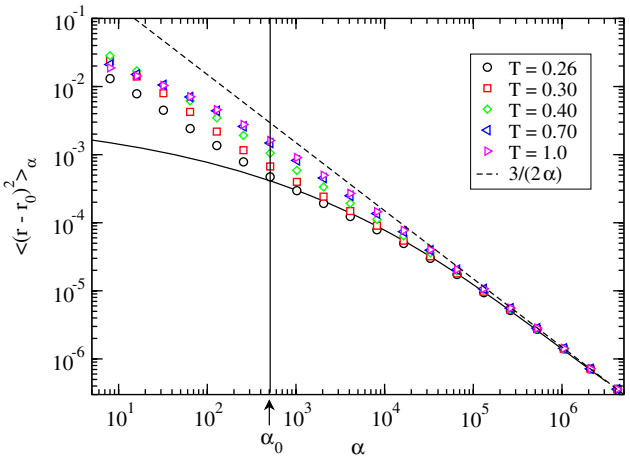

Figure 10. $\langle(\mathbf{r} - \mathbf{r}_0)^2\rangle_\alpha$ at different temperatures as a function of α on a logarithmic scale.

4.3. Configurational entropy

We are now able to estimate the configurational entropy. The two routes described above give rise to two different estimations of S_{conf}. Let us start with S_{conf} calculated using PEL vibrational entropy. Figure 12(a) shows the configurational entropy per particle $S^{(1)}_{\mathrm{conf}}/N$, calculated as the difference between total entropy expressed by equation (9) and vibrational entropy $S^{(1)}_{\mathrm{vib}}$ given by equation (10). The T-dependence shows a well defined maximum at temperature $T^{(1)}_{\mathrm{max}} \simeq 0.6$, slightly higher than that of diffusivity ($T_{\mathrm{max}} = 0.4$). The presence of the maximum is a remarkable result, indicating a close relationship between the temperature dependence of diffusivity and configurational entropy, even if a quantitative coincidence of the peaks seems not to be exactly achieved. Of course, the use of the harmonic

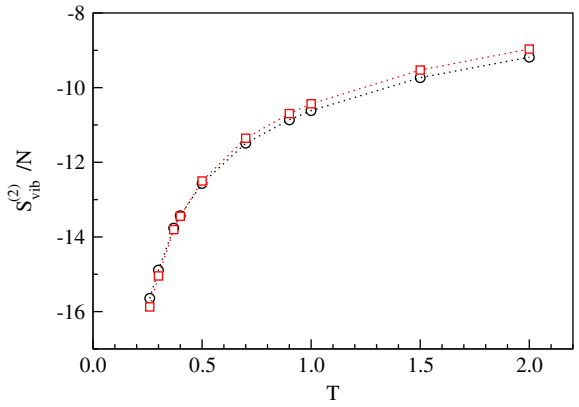

Figure 11. Vibrational entropy as a function of temperature (perturbed Hamiltonian approach). Circles are obtained adding a constant (T-independent) term $c = 0.4$ in equation (16), while squares are obtained using a T-dependent extrapolation (see text for details).

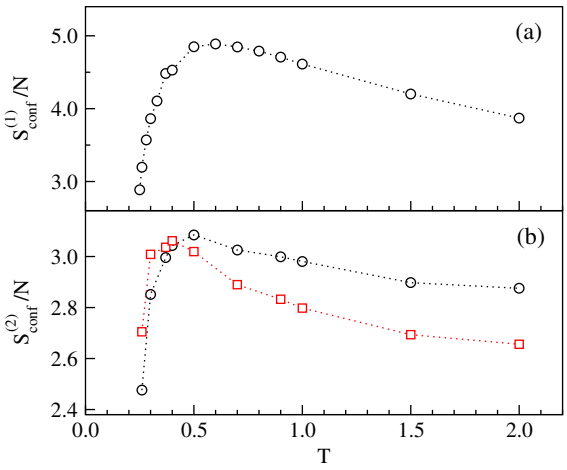

Figure 12. Configurational entropy as a function of temperature calculated using the PEL approach (panel (a)) and the perturbed Hamiltonian approach (panel (b)). Circles and squares in panel (b) correspond to the two extrapolated $\alpha = 0$ contributions in the calculation of $S^{(2)}_{vib}$ (see figure 11).

approximation deserves a few remarks: while in the simple liquid the harmonic approximation works well at sufficiently low T, in our case, due to the steepness of the pair potential, the harmonic approximation is expected to break down at a much lower T. It is worth noting that an estimation of the anharmonic contributions, following the techniques developed for atomic and molecular systems, is not feasible in the present case due to the strong T-dependence of the anharmonic energy. Moreover, due to the fact that at high T the confining cage is not controlled by the short range attractive interaction but by the excluded volume, the caging emerges from an averaging over many different inherent structures, invalidating the use of a single potential energy minimum to infer vibrational properties. For these reasons a different method is needed to corroborate the above findings. The alternative method for the calculation of S_{conf} is given by the perturbed Hamiltonian approach. Figure 12(b) shows the T-dependence of the configurational entropy per particle $S^{(2)}_{conf}/N$, calculated as the difference between total entropy and $S^{(2)}_{vib}$. As the latter has been estimated using two extrapolated procedures (see figure 11), we also obtain two estimations of $S^{(2)}_{conf}$ (circles and squares in figure 12, accordingly to the symbols in figure 11). Again one observes a peak, located at about $T^{(2)}_{max} \simeq 0.4$–0.5, closed to that of diffusivity. We note that using the same value of α_0 for all the temperatures introduces an underestimation of $S^{(2)}_{vib}$, more pronounced for the high T data. This fact could have the effect of moving the peak to a lower T value, approaching the peak value of the diffusivity. Although the absolute values of $S^{(1)}_{conf}$ and $S^{(2)}_{conf}$ are different (as said before, possible causes of this discrepancy are over- or under-estimations due to anharmonicity effects in the PEL approach or to the choice of α_0 and the extrapolating function in the Perturbed approach) the T-dependence is quite similar, suggesting that the errors are mostly T-independent. More interestingly, in both approximations a maximum in S_{conf}, not far from the T at which D has a maximum, is clearly detected. Since both methods give a T-dependence of the configurational entropy with a peak located close to that of diffusivity, our work strongly supports the possibility that in short range colloidal systems the diffusivity maximum is related to a maximum in the number of states visited by the system.

5. Conclusions

In conclusion, we have introduced a continuous pair potential model describing short ranged attractive colloids, generalizing a $2n - n$ Lennard-Jones potential with $n = 100$. We have analyzed static and dynamic quantities (static structure factors, mean square displacements, diffusivity, self-correlation functions, relaxation times) as a function of temperature at fixed high density. In agreement with previous theoretical, numerical and experimental studies, we found the presence of a peak in the diffusivity (and in the inverse relaxation times), confirming for our model the existence of two slowing down regions at low and high temperature, respectively. We have then investigated the possible relationship between diffusivity and configurational entropy, looking for the existence of a similar peak in the S_{conf}. With this aim, we have followed two distinct ways of calculating S_{conf}, both using an estimation of the vibrational entropy term: the first one, based on the PEL approach, makes use of inherent structures properties, the second one, based on the Frenkel–Ladd method, adds a perturbed harmonic term in the Hamiltonian and then follows a suitable extrapolation to vanishing perturbation. The two estimations of S_{conf} show a quantitative difference in their absolute values, due to under- and/or over-estimation present in both methods (ascribed to the harmonic approximation in the PEL method, and to the choice of α_0 and/or the choice of the extrapolating function to low α values for the perturbed Hamiltonian method). However, even though both methods make use of some approximation, we found the remarkable fact that both give rise to a peak in the S_{conf} varying with T. The qualitative agreement between the T

behaviors is a strong argument for the robustness of the result: the configurational entropy and diffusivity show a maximum at the same temperature. Our findings strongly support the possibility that in short range attractive colloidal systems the diffusivity peak is related to a maximum in the number of states explored by the system.

Acknowledgments

We thank F Sciortino for useful discussions. GF acknowledges the support of the Swiss National Science Foundation (grant no. 200021-105382/1).

References

[1] Hoover W G and Ree F H 1968 *J. Chem. Phys.* **49** 3609
[2] Pusey P N and van Megen W 1986 *Nature* **320** 340
[3] Likos C N 2001 *Phys. Rep.* **348** 267
[4] Gast A P, Russell W B and Hall C K 1983 *J. Colloid Interface Sci.* **96** 251
[5] Meijer E and Frenkel D 1991 *Phys. Rev. Lett.* **67** 1110
[6] Anderson V J and Lekkerkerker H N W 2002 *Nature* **416** 811
[7] Pusey P N 1991 *Liquids, Freezing and Glass Transition* (*Les Houches Summer Schools of Theoretical Physics* vol Session LI (1989)) ed J P Hansen, D Levesque and J Zinn-Justin (Amsterdam: North-Holland) pp 765–942
[8] Götze W 1991 *Liquids, Freezing and Glass Transition* (*Les Houches Summer Schools of Theoretical Physics* vol Session LI (1989)) ed J P Hansen, D Levesque and J Zinn-Justin (Amsterdam: North-Holland) pp 287–503
[9] van Megen W and Underwood S M 1993 *Phys. Rev. Lett.* **70** 2766
[10] Fabbian L, Götze W, Sciortino F, Tartaglia P and Thiery F 1999 *Phys. Rev.* E **59** R1347
[11] Fuchs M and Müller M 1999 *Phys. Rev.* E **60** 1921
[12] Dawson K A, Foffi G, Fuchs M, Götze W, Sciortino F, Sperl M, Tartaglia P, Voigtmann T and Zaccarelli E 2001 *Phys. Rev.* E **63** 11401
[13] Pham K N, Puertas A M, Bergenholtz J, Egelhaaf S U, Moussaïd A, Pusey P N, Schofield A B, Cates M E, Fuchs M and Poon W C K 2002 *Science* **296** 104
[14] Chen S-H, Chen W-R and Mallamace F 2003 *Science* **300** 619
[15] Puertas A M, Fuchs M and Cates M E 2002 *Phys. Rev. Lett.* **88** 98301
[16] Foffi G, Dawson K A, Buldyrev S V, Sciortino F, Zaccarelli E and Tartaglia P 2002 *Phys. Rev.* E **65** 050802(R)
[17] Zaccarelli E, Foffi G, Sciortino F and Tartaglia P 2003 *Phys. Rev. Lett.* **91** 108301
[18] Scala A, Starr F, Nave E L, Sciortino F and Stanley H 2000 *Nature* **406** 166
[19] Debenedetti P G and Stillinger F H 2001 *Nature* **410** 259
[20] Wales D 2004 *Energy Landscapes: Applications to Clusters, Biomolecules and Glasses* (Cambridge: Cambridge University Press)
[21] Sastry S 2001 *Nature* **409** 164
[22] Angelani L, Foffi G, Sciortino F and Tartaglia P 2005 *J. Phys.: Condens. Matter* **17** L113
[23] Vliegenthart G A, Lodge J and Lekkerkerker H N W 1999 *Physica* A **263** 378
[24] Allen M P and Tildesley D J 1989 *Computer Simulation of Liquids* (Oxford: Clarendon)
[25] Bergenholtz J and Fuchs M 1999 *Phys. Rev.* E **59** 5706
[26] Zaccarelli E, Foffi G, Dawson K A, Buldyrev S V, Sciortino F and Tartaglia P 2002 *Phys. Rev.* E **66** 41402
[27] Hansen J-P and McDonald I R 1986 *Theory of Simple Liquids* 2nd edn (London: Academic)
[28] Gleim T, Kob W and Binder K 1998 *Phys. Rev. Lett.* **81** 4404
[29] Franosch T, Fuchs M, Götze W, Mayr M R and Singh A P 1997 *Phys. Rev.* E **55** 7153
[30] Foffi G, Michele C D, Sciortino F and Tartaglia P 2005 *J. Chem. Phys.* **122** 224903
[31] Puertas A, Fuchs M and Cates M 2007 *Phys. Rev.* E **75** 031401
[32] Foffi G, Götze W, Sciortino F, Tartaglia P and Voigtmann T 2004 *Phys. Rev.* E **69** 11505
[33] Sperl M 2003 *Phys. Rev.* E **68** 31405
[34] Mallamace F, Gambadauro P, Micali N, Tartaglia P, Liao C and Chen S-H 2000 *Phys. Rev. Lett.* **84** 5431
[35] Götze W and Sperl M 2002 *Phys. Rev.* E **66** 11405
[36] Puertas A M, Michele C D, Sciortino F, Tartaglia P and Zaccarelli E 2007 *J. Chem. Phys.* **127** 144906
[37] Krekelberg W, Mittal J, Ganesan V and Truskett T 2007 *J. Chem. Phys.* **127** 044502
[38] La Nave E, Sciortino F, Tartaglia P, Michele C D and Mossa S 2003 *J. Phys.: Condens. Matter* **15** S1085
[39] Sciortino F, Kob W and Tartaglia P 1999 *Phys. Rev. Lett.* **83** 3214
[40] Rosenfeld Y and Tarazona P 1998 *Mol. Phys.* **95** 141
[41] Stillinger F and Weber T 1984 *Science* **225** 983
[42] Broderix K, Bhattacharya K, Cavagna A, Zippelius A and Giardina I 2000 *Phys. Rev. Lett.* **85** 5360
[43] Sastry S, Debenedetti P and Stillinger F 1998 *Nature* **393** 554
[44] Chakraborty S and Chakravarty C 2006 *J. Chem. Phys.* **124** 014507
[45] Keyes T 1997 *J. Phys. Chem.* A **101** 2921
[46] Frenkel D and Smit B 2001 *Understanding Molecular Simulation* 2nd edn (London: Academic)
[47] Coluzzi B, Mezard M, Parisi G and Verrocchio P 1999 *J. Chem. Phys.* **111** 9039
[48] Angelani L and Foffi G 2007 *J. Phys.: Condens. Matter* **19** 256207
[49] Moreno A J, Buldyrev S V, Nave E L, Saika-Voivod I, Sciortino F, Tartaglia P and Zaccarelli E 2005 *Phys. Rev. Lett.* **95** 157802
[50] Foffi G and Sciortino F 2006 *Phys. Rev.* E **74** 050401